Diamond & Related Materials 92 (2019) 187–197

Contents lists available at ScienceDirect

Diamond & Related Materials

journal homepage: www.elsevier.com/locate/diamond

Effects of bilayer number and thickness ratio on structure and properties of (Cr, N)-DLC/DLC multilayer films

Chaoqian Guo[a], Zhiliang Pei[b,*], Jun Gong[b], Chao Sun[b,*], Songsheng Lin[a], Qian Shi[a]

[a] Guangdong Institute of New Materials, National Engineering Laboratory for Modern Materials Surface Engineering Technology, The Key Lab of Guangdong for Modern Surface Engineering Technology, Guangzhou 510651, China
[b] Institute of Metal Research, Chinese Academy of Sciences, Shenyang 110016, China

ARTICLE INFO

Keywords:
Diamond-like carbon
Multilayer
Bilayer number
Thickness ratio
Properties
Arc

ABSTRACT

(Cr, N)-DLC/DLC multilayer films with different bilayer numbers and thickness ratios were prepared on cemented carbides and silicon wafers by cathodic vacuum arc technology. Surface and cross-section morphologies of multilayer films were observed by scanning electron microscope. Roughness, hardness, adhesion strength, friction coefficient and wear rates of the deposited films were investigated by surface profiler, nanoindentor, scratch tester, and ball-on-disk tribometer, respectively. Alternating stress field from adjacent sublayers benefited the mechanical properties while macroparticles piercing through interfaces between sublayers provided passages for cracks propagation and deteriorated films' mechanical properties. As bilayer numbers varied from 10 to 20 average friction coefficient and roughness of multilayer films had the same changing trend and wear rates increased linearly from 2.45×10^{-7} mm^3/Nm to 3.81×10^{-7} mm^3/Nm. Improving proportion of (Cr, N)-DLC layer in multilayer films increased quantity of macroparticles, leading to the rise of multilayer films' roughness, average friction coefficient and wear rates.

1. Introduction

Diamond-like carbon (DLC) film is a kind of amorphous carbon film containing sp^2 bonds and sp^3 bonds [1–4]. DLC film attracts attentions from not only scientists but also engineers due to its fascinating properties [5–8], such as high hardness, low friction coefficient, excellent wear resistance, good thermal conductivity, making DLC and its related materials one of the most-studied coatings [2,9–12]. However, high compressive residual stress in DLC film makes it easy to generate cracks and even peel off substrate, limiting its applications [13–16]. Multilayer structural design is an effective method of relieving residual stress, improving film's thickness and extending lifespan of workpieces with DLC films [17–20].

Period of multilayer and thickness ratio of one monolayer to another are key factors in regulating multilayer film's properties. Zhu et al. [21] investigated the influence of modulation period on structure, morphology, mechanical properties and tribological behaviors in different environments of Si/a-C:H multilayer films deposited by radio-frequency magnetron sputtering. Content of sp^2 hybrid carbon, surface roughness and hardness of the multilayer film changed with modulation period and further affected film's tribological behavior. Morphology, structure, composition, mechanical and tribological properties of DLC/MoS_2 multilayer coatings with different modulus ratios prepared by magnetron sputtering were studied in the research of Zhao et al. [22]. Cui et al.'s article [23] showed that corrosion resistance of the silicon doped multilayer DLC coatings was significantly improved with the increase of deposition periods. DLC/TiC multilayer films' residual stress was effectively reduced with the modulation period decreasing and hardness of film increased, on the contrary [24]. Increase of the proportion of hard layer in DLC film consisting of alternate soft-layer and hard-layer improved film's residual stress, hardness and reduced modulus [25]. Effect of modulation ratios on structure and properties of multilayer WS_x/a-C films [26], TiAlN/CrN coatings [27], CrAlN/VN coatings [28] and TiB_2/Al_2O_3 films [29] were also reported. Alternate (Cr, N)-DLC/DLC multilayer films with 5 bilayers and thickness ratio of 1:1 were investigated in the authors' previous research [30]. As bilayer number and thickness ratio varies, structure and properties of (Cr, N)-DLC/DLC multilayer films will of course change correspondingly.

In the present study, (Cr, N)-DLC/DLC multilayer films with different bilayer numbers (10, 15 and 20) and thickness ratios (2:1 and 4:1) of (Cr, N)-DLC layer to DLC layer were prepared on cemented carbides and silicon wafers by cathodic vacuum arc technology. Much attention was paid to the effect of bilayer number and thickness ratio on multilayer films' structure and tribomechanical properties.

* Corresponding authors.
E-mail addresses: zlpei@imr.ac.cn (Z. Pei), csun@imr.ac.cn (C. Sun).

https://doi.org/10.1016/j.diamond.2019.01.003
Received 27 September 2018; Received in revised form 7 January 2019; Accepted 8 January 2019
Available online 09 January 2019

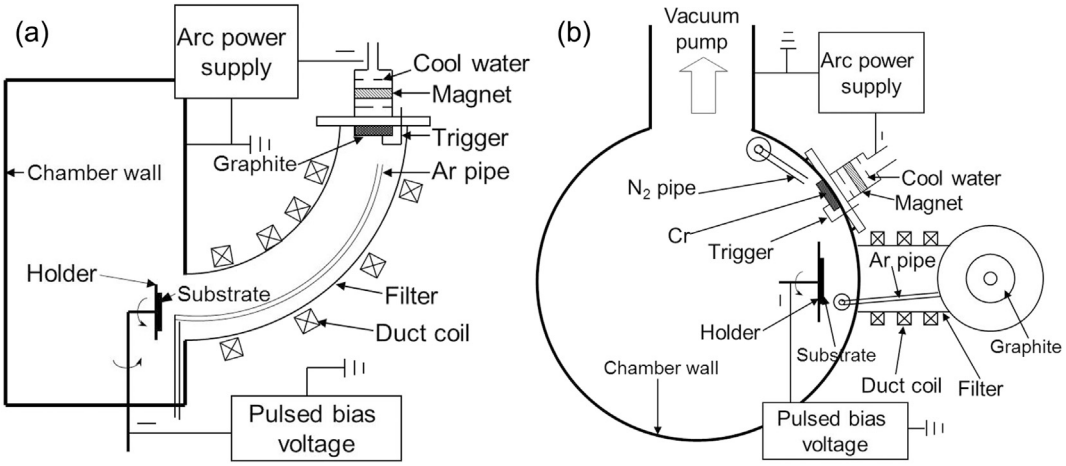

Fig. 1. (a) Cross-sectional and (b) top-view schematic of the deposition system [30].

Strengthening effects of interfaces between sublayers and increasing proportion of (Cr, N)-DLC layer in multilayer film benefit improving multilayer film's properties while macroparticles in films provide passages for cracks propagation, deteriorating film's properties.

2. Experimental details

2.1. Film deposition

(Cr, N)-DLC/DLC multilayer films with different bilayer numbers and thickness ratios between (Cr, N)-DLC layer and DLC layer were prepared on cemented carbides (YG8) and single-crystal silicon wafers by filtered combined with direct cathodic vacuum arcs. YG8 substrates with a mirror finished surface and Si wafers were ultrasonically cleaned in acetone and ethanol for 15 min, respectively, before film deposition. Schematic of the deposition system was shown in Fig. 1 [30]. A graphite target (99.9%) was mounted at the position of filtered cathodic vacuum arc source to provide carbon plasma while Cr plasma generated by direct cathodic vacuum arc source reached substrates surface under oblique incidence.

CrN layer with the thickness of about 100 nm acted as intermediate layer between (Cr, N)-DLC/DLC bilayers and substrate. Detailed deposition parameters were presented in Table 1. Throughout the deposition process, duty ratio and repetition frequency of bias voltage were 15% and 50 kHz, respectively. Rotation speed of substrate holder was 10 rpm. The structure of (Cr, N)-DLC layer is a kind of composite structure containing amorphous phase and a small quantity of nanocrystalline compounds of chromium.

In the-present paper, multilayers with different bilayer numbers and thickness ratios presented in Table 2 were obtained by varying deposition time of each monolayer. Thicknesses of multilayer films were approximately 2 μm in which a CrN intermediate layer of about 100 nm was contained.

2.2. Film characterization

Surface and cross-sectional morphology as well as thickness of films were observed by field emission scanning electron microscope (SEM, Inspect F50, FEI, USA) with energy dispersive spectrometer (EDS). Percentage of macroparticles in a SEM photograph was calculated by Image pro-plus (IPP) software. Line roughness of films was measured by a surface profiler (Alpha-Step IQ, KLA Tencor). Each sample was measured three times with a scanning speed 50 μm.

Hardness and elastic modulus of multilayer films were investigated by a nano-indentation tester (Nano indentor G200, Agilent Technologies, USA) with a Berkovich indenter tip under the continuous stiffness mode (CSM). To avoid the effects of substrates, values of hardness and elastic modulus were obtained from the range of 10% of film thickness [31]. Ten repeated measurements were applied on each sample. In addition, elastic recovery W_e could be obtained from the load/unload-displacement curve [32]. Given that the maximum depth of indentations was about 450 nm which far exceeded 10% of film thickness, values of W_e represents the film-substrate system's elastic recovery capacity. However, considering the same substrates and film thicknesses, W_e can still reflect mechanical properties of multilayer films with different structures. Elasticity (R) of multilayer films were calculated according to formula $R = (h_{max} - h_r) / h_{max}$, in which h_{max} was the maximum value of displacement during indenter loading and h_r stood for the remaining value of displacement after indenter unloaded.

Scratch tests were performed by MFT-4000 multifunction material surface tester with a Rockwell diamond indenter to characterize the adhesion strength between films and substrates. Scratch speed was 10 mm/min at a loading rate of 100 N/min. Scratch morphologies on multilayer films were observed by an optical microscope Carl Zeiss Axio Observer Z1m. Ball-on-disk tribometer MS-T3000 was used to measure friction coefficient of multilayer films on YG8 substrates in ambient atmosphere (approx. 20% humidity) at room temperature (20 °C). Counterparts were Al_2O_3 balls which had diameters of 4 mm. Friction tests were carried out at rotation speed of 200 rpm under normal load of 2 N with wear time of 4 h. Surface morphologies and profiles of wear tracks were measured by the optical microscope and surface profiler, respectively. Multilayer films' wear rates were also calculated according to the Archard equation $W = V / (S \times L)$, where V is wear volume, S is

Table 1
Deposition parameters of CrN, (Cr, N)-DLC, DLC monolayers.

Monolayer	Negative bias voltage (V)	Work pressure (Pa)	Deposition rate (nm/min)
CrN	400	0.7	≈10
(Cr, N)-DLC	400	0.4	≈26
DLC	500	0.1	≈36

Table 2
Bilayer numbers and thickness ratios of (Cr, N)-DLC/DLC multilayer films.

Sample no.	Bilayer numbers	Thickness ratios [(Cr, N)-DLC:DLC]
B10	10	1:1
B15	15	
B20	20	
R2	10	2:1
R4		4:1

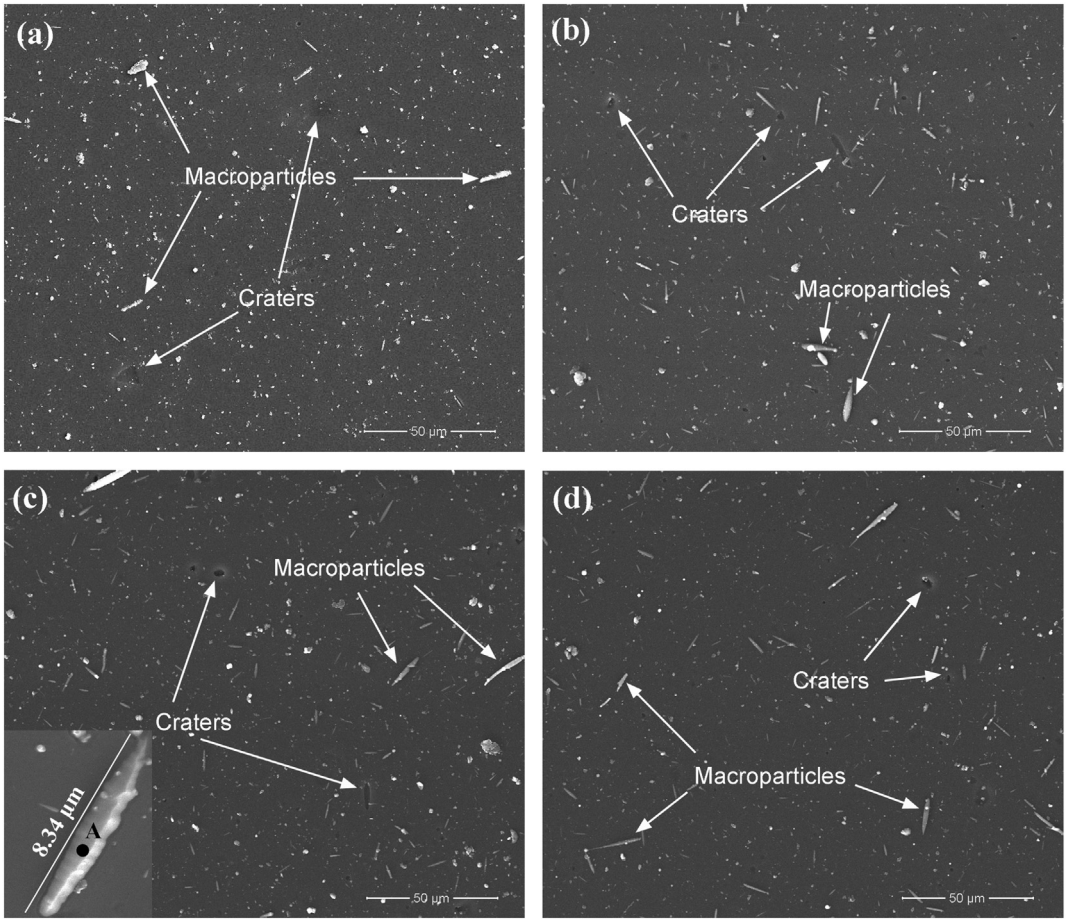

Fig. 2. SEM surface morphologies of (Cr, N)-DLC/DLC multilayers with different bilayer numbers: (a) 5 bilayers, (b) 10 bilayers, (c) 15 bilayers, (d) 20 bilayers.

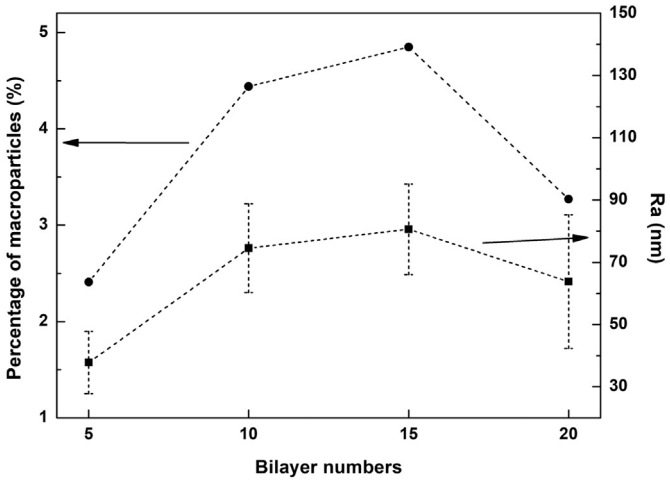

Fig. 3. Percentage of macroparticles and roughness (Ra) of (Cr, N)-DLC/DLC multilayers as bilayer number changes.

sliding distance, and *L* is applied load.

3. Results and discussion

3.1. Effect of bilayer number on multilayer films' morphology and properties

In order to clarify the effect of bilayer number on structure of multilayer films, some research data of sample 5 composed of 5 (Cr, N)-DLC/DLC bilayers with the thickness ratio of 1:1 ((Cr, N)-DLC layer to DLC layer) prepared in previous research [30] is also displayed in the-present article.

Surface morphology of (Cr, N)-DLC/DLC multilayer films with different bilayer numbers were investigated by SEM shown in Fig. 2. Macroparticles with the shape of spindle can be observed as well as craters formed by macroparticles falling off. The inset in Fig. 2c is an enlarged image of a macroparticle with the size of 8.34 μm. Atomic contents of Cr and N elements in point A analyzed by EDS are 53.1% and 46.9%, respectively. During the deposition process, Cr droplets flew from target to substrates which had a lower temperature than chromium melting point [33] at a certain angle and then solidified on the surface of substrates. Because of the effect of inertia, Cr macroparticles presented the shape of spindle with a thick end and a thin end. As for craters, two reasons contribute to their formation. On the one hand, the composition and structure of macroparticles are different from that of film which leads to different thermal expansion coefficients. After the deposition process finished, substrates temperature declined from more than one hundred degrees Celsius [30] to room temperature. Macroparticles fell off from multilayer films due to different shrinking states. On the other hand, macroparticles were bombarded by ions and atoms throughout the deposition procedure. Bombardments conduced to the drop-out of macroparticles giving rise to the formation of craters.

In Fig. 3, circles linked by a dotted line are percentages of macroparticles on SEM photographs with different bilayer numbers calculated via IPP software which are in the range of 2.41%–4.85% while squares linked by a dotted line represent surface roughness (Ra) of multilayers. Percentages of macroparticles and Ra have the same trends that the maximum value appears as bilayer number is 15 and the minimum value appears as bilayer number is 5. Emission rate of macroparticles is

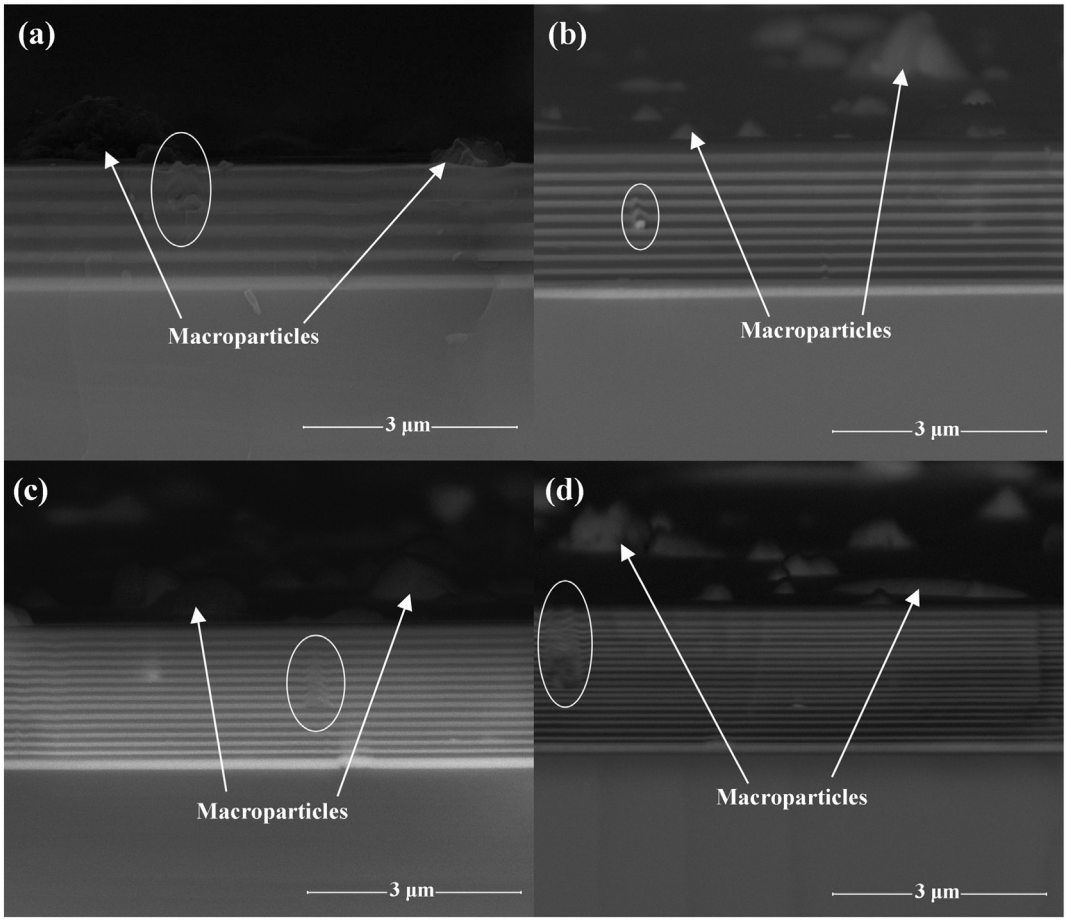

Fig. 4. SEM cross-section morphologies (in BSE mode) of (Cr, N)-DLC/DLC multilayers with different bilayer numbers: (a) 5 bilayers, (b) 10 bilayers, (c) 15 bilayers, (d) 20 bilayers.

mainly affected by two reasons: arc current and cathode surface temperature [34]. Peak emission rate of macroparticles follows the peak value of arc current at either 6 or 1 ms after arc initiation [35]. That is, quantity of macroparticles on multilayer film's surface increased with the number of arc initiation which increased with the bilayer number in multilayer films. On the other hand, continuous discharging of arc target produced lots of Joule heat resulting in much more macroparticles. The rise of bilayer number meant reducing continuous discharging time of chromium and graphite targets which benefited heat releasing of targets' surface and decreasing quantity of macroparticles. Under the combined action of the two factors, quantity of macroparticles and Ra increased at first and declined subsequently as bilayer number rose from 5 to 20.

Fig. 4 illustrates cross-section morphologies of (Cr, N)-DLC/DLC multilayers with different bilayer numbers in backscattered electron (BSE) mode. In BSE imaging mode, the brighter area denotes the existence of much heavier atoms. Therefore, the layer next to substrate which has the highest brightness is intermediate layer CrN with the thickness of about 100 nm. The adjacent layer which has the lower brightness is (Cr, N)-DLC and the darkest layer is DLC. Total thicknesses of multilayers are about 2 μm. Thicknesses of monolayers in multilayer films with 5, 10, 15 and 20 bilayers were approximately 170 nm, 94 nm, 63 nm and 47 nm, respectively. Furthermore, macroparticles having much higher brightness than areas around them also proved that macroparticles were mainly from chromium target, due to the much larger atomic number of chromium than that of carbon. Meanwhile, macroparticles circled by ellipses in Fig. 4 could be seen embedding in multilayer films.

Table 3 exhibits the hardness, elastic modulus, elastic recovery (W_e) and elasticity (R) of (Cr, N)-DLC/DLC multilayer films. As bilayer numbers increase from 10 to 20, mechanical parameters displayed in Table 3 change slightly. Hardness of samples B10, B15 and B20 is approximately 19 GPa and elastic moduli are in the range of 235 GPa to 255 GPa as W_e values are close to 0.50. Hardness, elastic modulus and W_e value of multilayer film with 5 bilayers are 14.38 GPa, 160.58 GPa and 0.47, respectively [30]. That is, mechanical properties of (Cr, N)-DLC/DLC multilayer films have been improved as bilayer number increased from 5 to 10, 15 and 20.

Table 3
Hardness, elastic modulus, W_e and elasticity (R) of samples B10, B15 and B20.

Sample no.	Hardness (GPa)	Elastic modulus (GPa)	W_e	R (%)
B10	19.05 ± 2.10	246.36 ± 29.26	0.51 ± 0.01	48.90 ± 1.66
B15	19.05 ± 0.64	250.25 ± 9.85	0.50 ± 0.01	48.99 ± 0.69
B20	18.90 ± 0.81	238.61 ± 11.63	0.49 ± 0.01	48.55 ± 1.10

Residual stresses in DLC layer and (Cr, N)-DLC layer were −1.59 GPa and −0.99 GPa, respectively [30]. Change of bilayer number of multilayers means that alternating stress field in multilayers varied. Xu et al. [36] thinks that alternating stress field caused by the two adjacent sublayers affects multilayer's hardness. Kodali et al. [37] addressed that crack initiation was affected by hardness and apparent fracture toughness of DLC coatings increased with coating hardness. Value of W_e represents film-substrate system's elastic recovery capacity which can also reflect toughness of the film. Compared with W_e of 0.47 of multilayer film with 5 bilayers, values of W_e of multilayer films with 10, 15 and 20 bilayers in the range of 0.49–0.51 were much higher

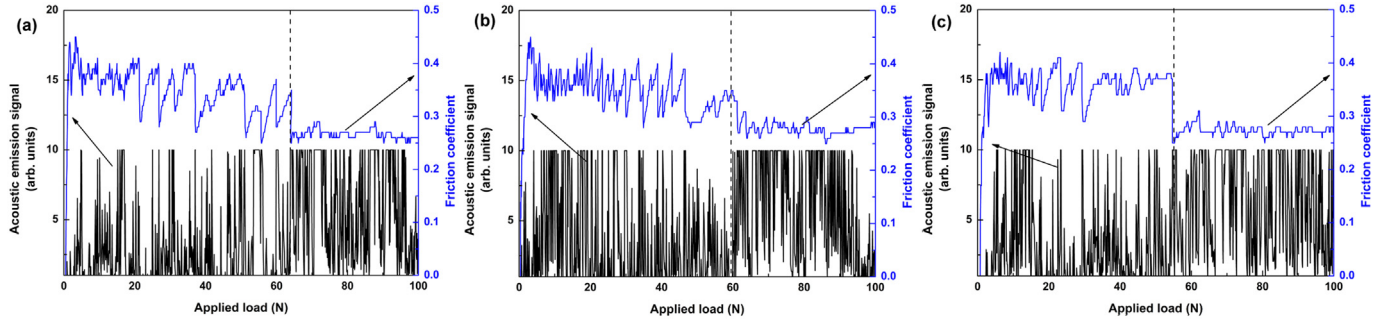

Fig. 5. Acoustic emission signal/friction coefficient-applied load curves of samples (a) B10, (b) B15, and (c) B20 obtained by scratch tests.

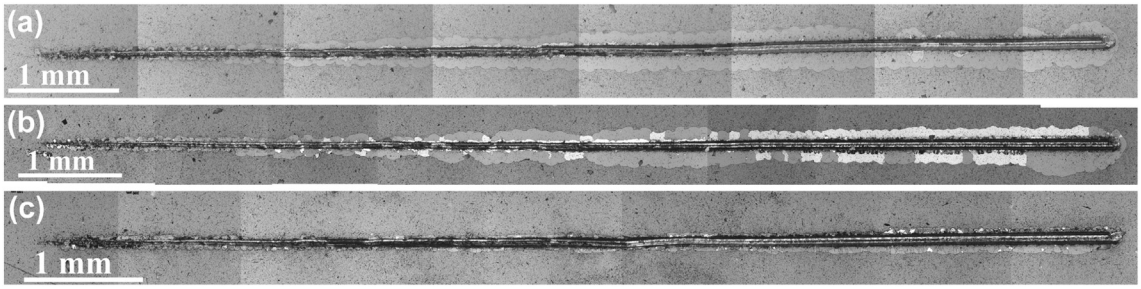

Fig. 6. Scratch morphologies of samples (a) B10, (b) B15, and (c) B20.

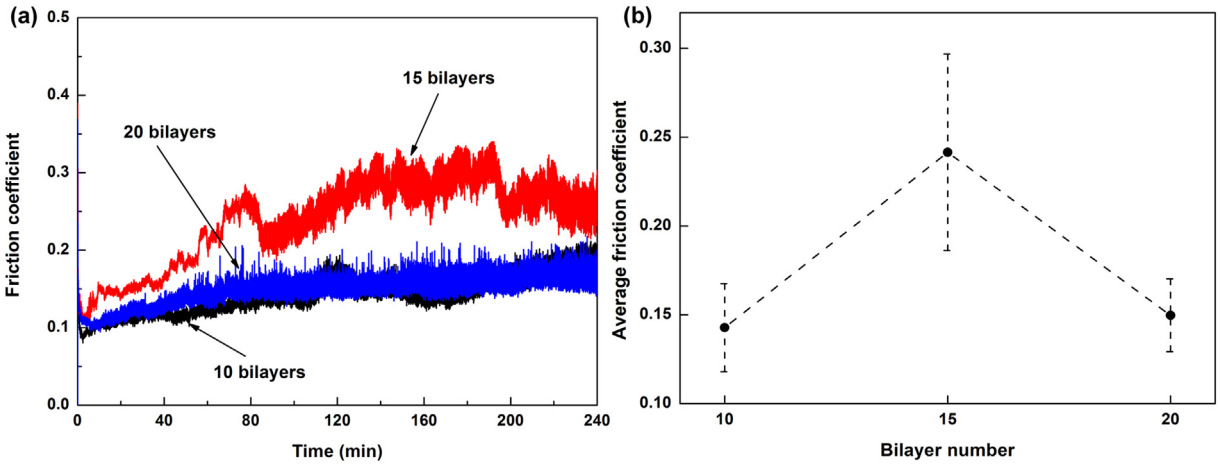

Fig. 7. (a) Friction coefficient and (b) average friction coefficient of samples B10, B15 and B20.

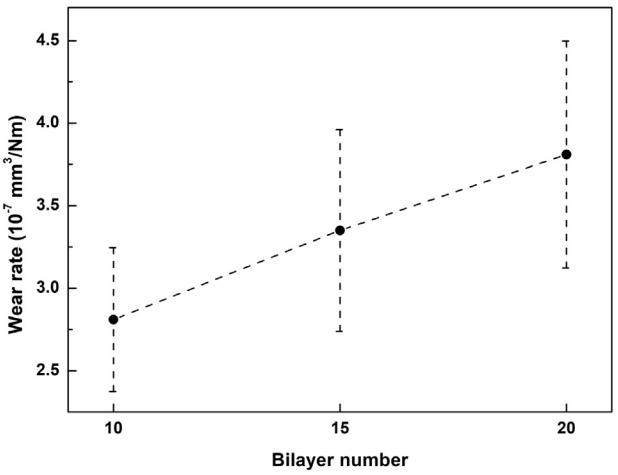

Fig. 8. Wear rates of (Cr, N)-DLC/DLC multilayer films with different bilayer numbers.

indicating a much better toughness caused by the increased hardness. At the same time, macroparticles piercing through one or more interfaces can be seen in Fig. 4 which may provide passages for cracks propagation and impair multilayer's mechanical properties. As bilayer number increased from 5 to 20 monolayers' thickness declined from 170 nm to 47 nm. Accordingly, more interfaces were transpierced by macroparticles which would go against multilayers' mechanical properties. On the other hand, macroparticles mainly comprised of Cr particles had big differences with films in mechanical properties and were distributed in films acting as flaws affecting films' properties. Therefore, mechanical properties of multilayer films went up as bilayer number increased from 5 to 10 and then reached a plateau as bilayer number rose from 10 to 20.

(Cr, N)-DLC/DLC multilayer films' adhesion strength was measured by scratch tests with a MFT-4000 multifunction material surface tester. Acoustic emission signal/friction coefficient-applied load curves are presented in Fig. 5. Friction coefficients of each multilayer sample fluctuated greatly accompanied by acoustic emission signal because indenter touched DLC monolayer and (Cr, N)-DLC monolayer

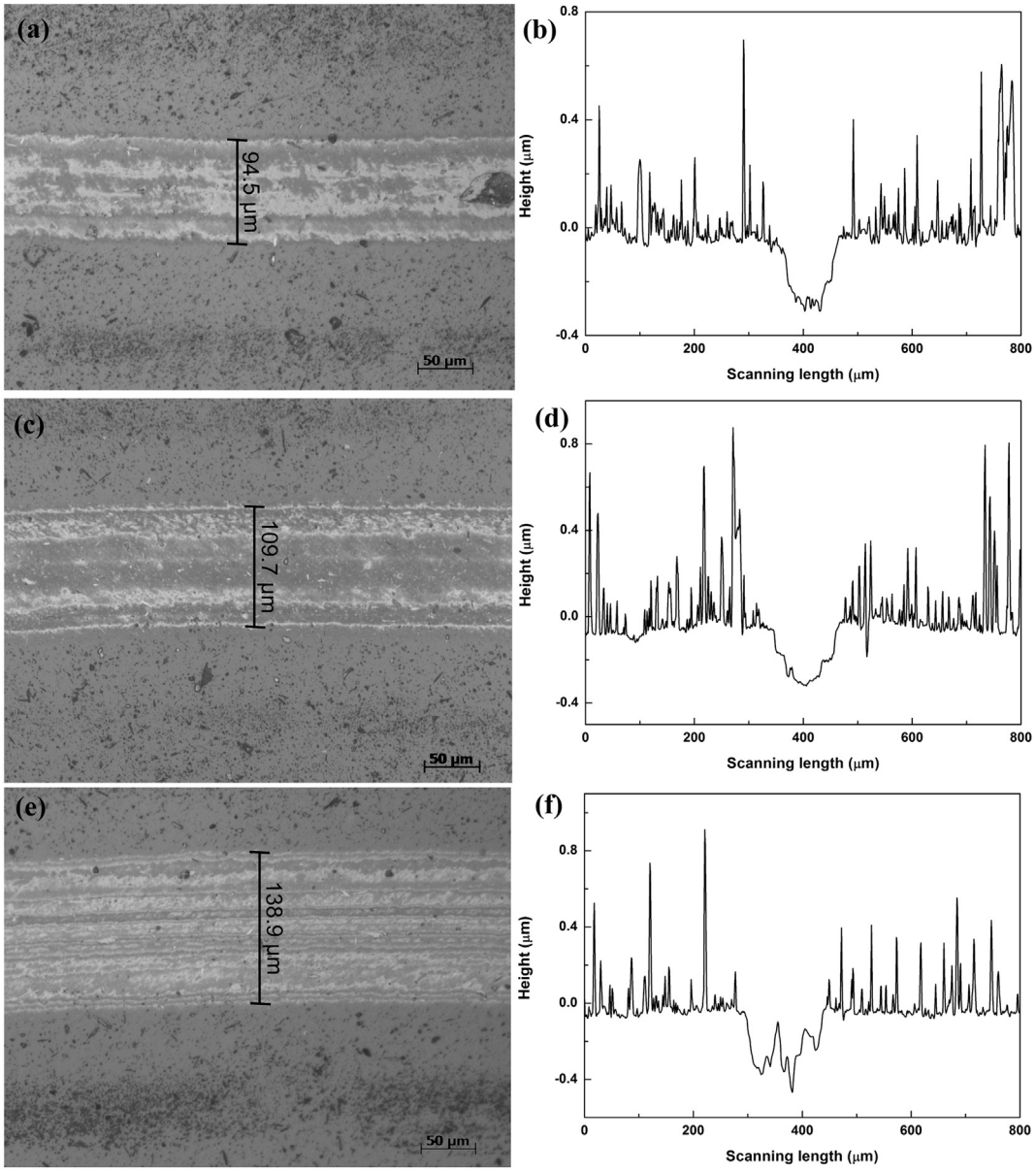

Fig. 9. Morphologies and profiles of wear tracks on (Cr, N)-DLC/DLC multilayer films: (a), (b) sample B10; (c), (d) sample B15; (e), (f) sample B20.

alternately as scratch depth increased. Saltation of friction coefficient and acoustic emission signal was marked by a dotted line. Scratch morphologies of samples B10, B15 and B20 were observed by an optical microscope indicated in Fig. 6. Although saltation of friction coefficient and acoustic emission signal is distinct, high critical loads are difficult to obtain from scratch images. Multilayer films on sample B15 flaked off more obviously than samples B10 and B20. Critical load is affected not only by the film's composition and structure but also film thickness, substrate's hardness and friction coefficient between film and indenter [38–40].

Fig. 7 presents friction coefficient of (Cr, N)-DLC/DLC multilayers with different bilayer numbers. Friction coefficient of samples B10 and B20 rose slightly but still lower than 0.2. As the extension of wear time, wear track became much wider and deeper which meant that contact area between grinding ball and multilayer film increased gradually and much more atoms were put away by grinding ball during each rotation of sample which gave rise to the increase of friction coefficient. As for sample B15, it exhibited a much higher and more variable friction coefficient than that of samples B10 and B20. In the former 80 min during wear test, friction coefficient increased from 0.1 to 0.27. During 80th to 140th min, friction coefficient dropped to 0.20 firstly and then rose gradually. During 140th to 190th min, friction coefficient reached a plateau of about 0.3. During the last 50 min, friction coefficient declined to 0.25. Friction coefficient of sample B15 changed periodically probably because of the multilayer film's periodical structure.

Average friction coefficients of samples B10, B15 and B20 are indicated in Fig. 7b. Sample B15 have the biggest average friction coefficient 0.24 and samples B10 and B20 have similar average friction coefficient values of about 0.15. Changing trend of average friction coefficient is similar to that of roughness. Sample B15 has the biggest Ra value and the most macroparticles on film surface. According to the results of EDS, composition of macroparticles is $Cr_{0.53}N_{0.47}$ which is similar to that of CrN. Friction coefficient of CrN films are in the range of 0.2–0.5 which is higher than that of DLC [41]. Macroparticles acted as obstacles while grinding ball slid on film surface, leading to the high average friction coefficient.

Wear rates of different multilayer films calculated via Archard formula are shown in Fig. 8. Wear rates increased linearly from 2.45×10^{-7} mm^3/Nm to 3.81×10^{-7} mm^3/Nm as bilayer number changed from 10 to 20. It can be seen from Fig. 3 that sample B15 has

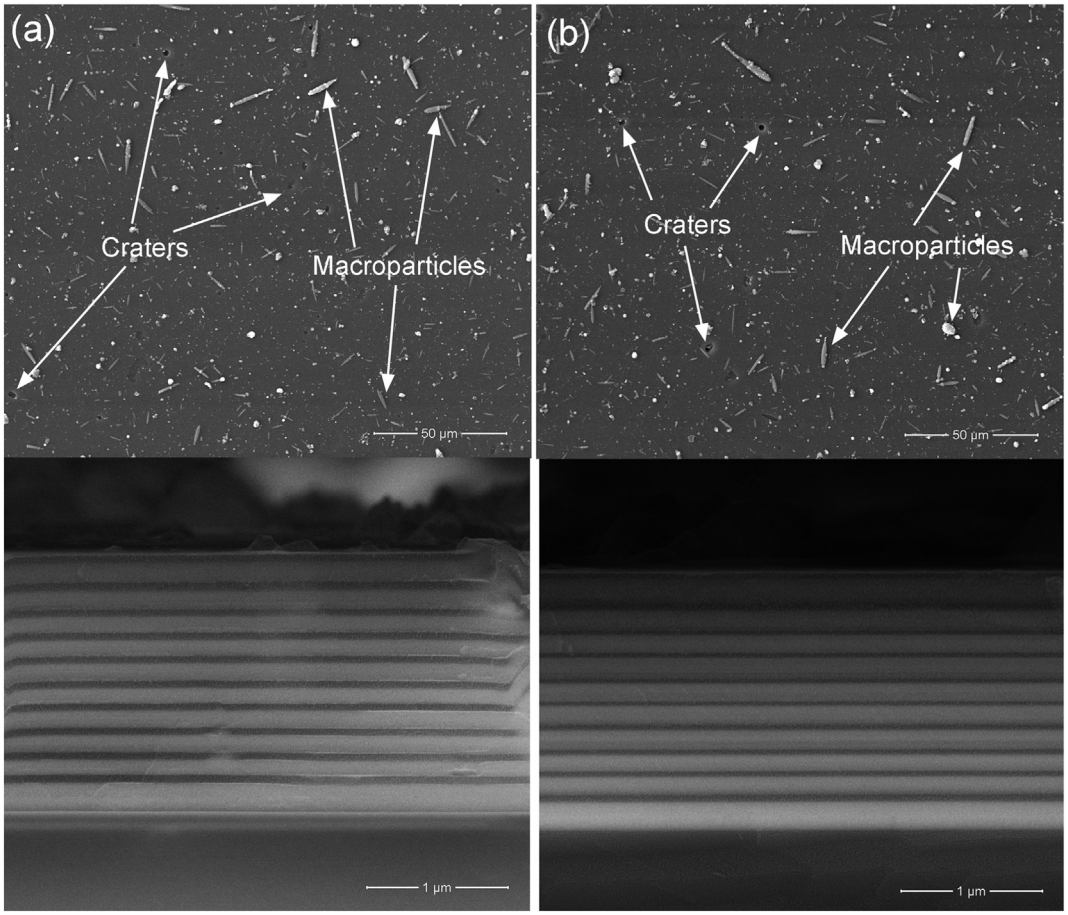

Fig. 10. Surface and cross-section morphologies of (Cr, N)-DLC/DLC multilayer films with different thickness ratios: (a) 2:1; (b) 4:1.

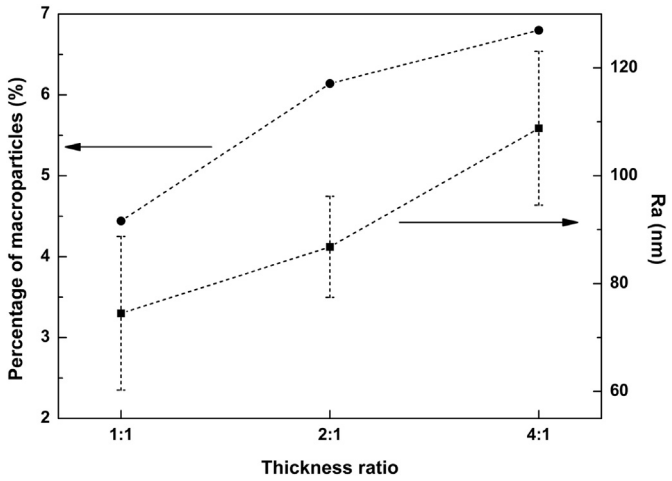

Fig. 11. Percentage of macroparticles and roughness (Ra) of (Cr, N)-DLC/DLC multilayer films with different thickness ratios.

much more macroparticles than sample B10. Macroparticles embedded in films deteriorated multilayers' mechanical properties causing the decline of films' wear resistance. In addition, the poor adhesion strength between macroparticles and multilayer film made macroparticles easy to drop out which also resulted in the increase of wear rate. However, wear rate of sample B20 with fewer macroparticles than sample B15 is much higher than that of sample B15. Monolayers in sample B20 is much thinner than that in sample B15. More interfaces in B20 were piercing though by macroparticles which may affect multilayer film's wear rate.

Surface morphologies and profiles of wear tracks on multilayer films are presented in Fig. 9 in which figures (a), (c) and (e) were captured by Carl Zeiss Axio Observer Z1m and figures (b), (d) and (f) were obtained from surface profiler. Width of wear tracks on multilayer films increased from 94.5 μm to 138.9 μm as bilayer number rose from 10 to 20. In Fig. 9a and c, wear tracks are smooth while "furrows" can be seen in wear tracks shown by Fig. 9e, indicating that abrasive wear existed between the counterpart ball and sample B20. Wear track depths on samples B10, B15 and B20 are 232 nm, 302 nm and 459 nm, respectively, read from wear track profiles. Wedge-shaped bulges at the bottom of wear track profiles in Fig. 9f are corresponding to the "furrows" observed in Fig. 9e. Wear track became much wider and deeper

Table 4
Hardness, elastic modulus, W_e and elasticity (R) of (Cr, N)-DLC/DLC multilayers with different thickness ratios.

Thickness ratio	Hardness (GPa)	Elastic (GPa)	W_e	R (%)
1:1	19.05 ± 2.10	246.36 ± 29.26	0.51 ± 0.01	48.90 ± 1.66
2:1	22.85 ± 1.67	300.34 ± 37.19	0.46 ± 0.01	46.28 ± 1.15
4:1	19.49 ± 1.32	250.43 ± 38.43	0.45 ± 0.01	44.73 ± 0.81

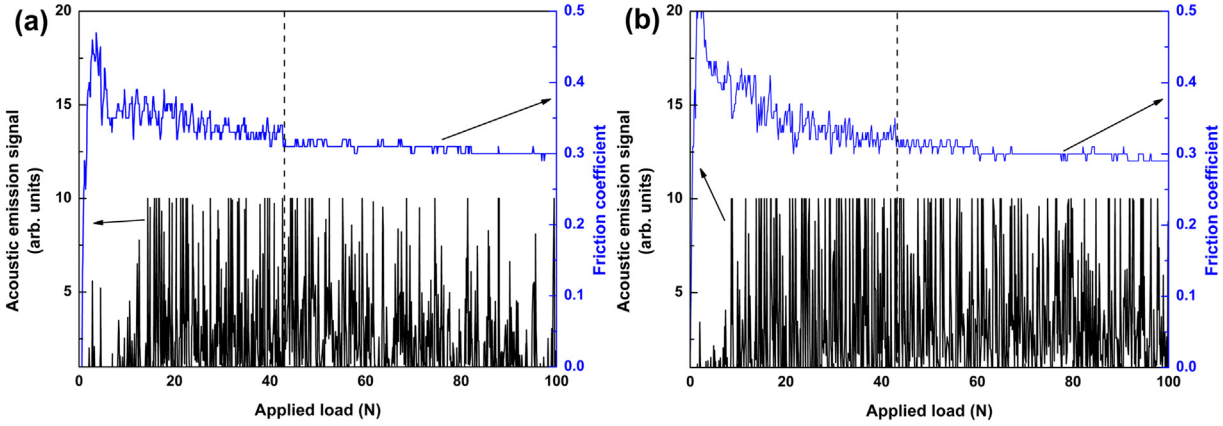

Fig. 12. Acoustic emission signal/friction coefficient-applied load curves of samples (a) R2 and (b) R4 obtained through scratch tests.

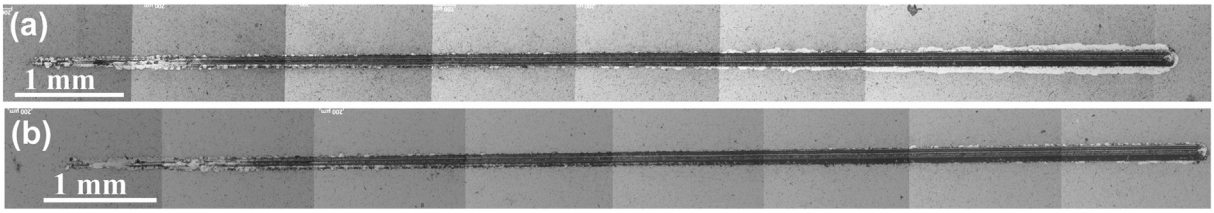

Fig. 13. Scratch morphologies of samples (a) R2 and (b) R4.

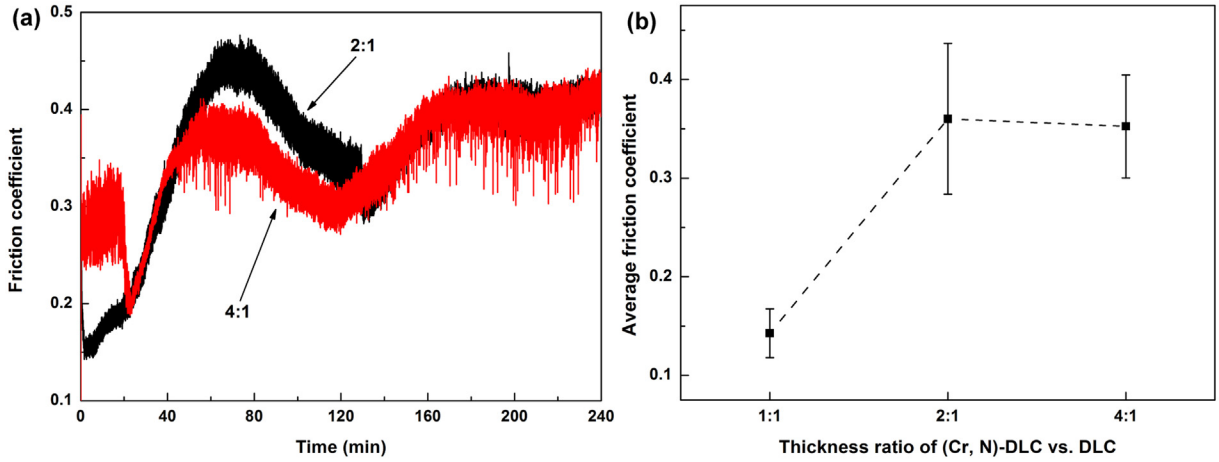

Fig. 14. (a) Friction coefficients of samples R2 and R4; (b) average friction coefficient of (Cr, N)-DLC/DLC multilayer films with different thickness ratios.

as bilayer number increased from 10 to 20, giving rise to a much higher wear rate.

As for sample B15, depth of wear track is 302 nm approximately 1.3 times thicker than the thickness of one (Cr, N)-DLC/DLC bilayer. That means two periodical bilayers have been worn out and the monolayer DLC in the third period is exposed to counterpart ball. Given the periodically changing friction coefficient displayed in Fig. 7, it took about 80 min to wear the first periodical bilayer out whereas it was about 110 min to grind off the second periodical bilayer. As wear test went on, contact area between grinding ball and multilayer film became much larger. Much more time was needed if grinding ball proceeded a certain distance into multilayer film because more atoms were stripped from wear track surface when normal load and rotation speed were invariable.

3.2. Effect of thickness ratio on multilayer films' morphology and properties

Surface and cross-section morphologies of (Cr, N)-DLC/DLC multilayer films with different thickness ratios (2:1 and 4:1) were studied by SEM in SE mode and BSE mode, respectively, presented in Fig. 10. Both craters and macroparticles can be observed on surface of multilayer films. Seen from the cross-section morphologies, ten periodical bilayers stack on substrates. The dark monolayer is DLC and the light monolayer is (Cr, N)-DLC. Total thicknesses of multilayer films are about 1.85 μm. In Fig. 10a (Cr, N)-DLC and DLC monolayers have the thicknesses of 120 nm and 57 nm, respectively, while in Fig. 10b thicknesses of (Cr, N)-DLC and DLC monolayers are 138 nm and 35 nm, respectively, which is corresponding with previous experimental design.

Percentage of macroparticles on samples R2 and R4 were calculated by IPP software which are 6.14% and 6.8%, respectively. Ra of multilayer films increased from 86.8 nm to 108.8 nm as thickness ratio rose from 2:1 to 4:1 as shown in Fig. 11. Changing trend of Ra is similar to that of percentage of macroparticles while thickness ratio increased. Macroparticles were mainly derived from Cr target. Improving the thickness of (Cr, N)-DLC layer would of course increase the content of

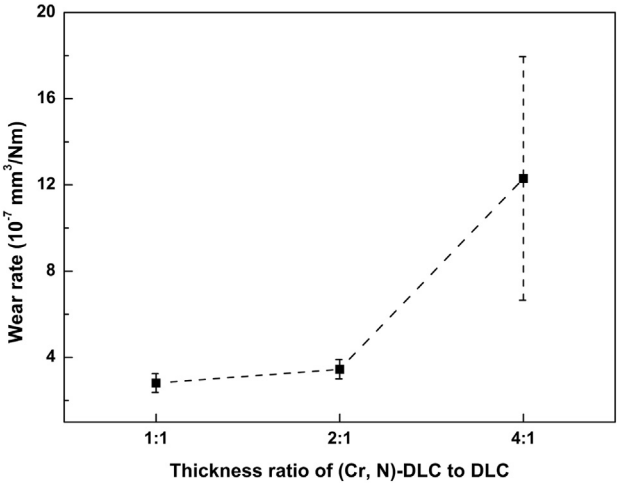

Fig. 15. Wear rates of (Cr, N)-DLC/DLC multilayer films with different thickness ratios.

macroparticles, causing the rise of roughness.

Hardnesses and elastic moduli of (Cr, N)-DLC/DLC multilayers with different thickness ratios measured by nanoindentor as well as W_e and elasticity (R) obtained from load/unload-displacement curve are displayed in Table 4. Hardness and elastic modulus of sample R2 have the largest values. Cr and N codoping into DLC leading to the carbides and nitrides of chromium [30] benefits hardness and elastic modulus of multilayer film while macroparticles acting as defects in multilayer films are bad for mechanical properties. Therefore, hardness and elastic modulus of multilayer film increased at first and then declined as thickness ratio increased from 1:1 to 4:1. Values of W_e and R are mainly affected by content of macroparticles. Increasing the total thickness of (Cr, N)-DLC layer in multilayer film gave rise to the decrease of W_e and R.

Fig. 12 illustrates the changing curves of acoustic emission signal and friction coefficient as indenter scratched on film surface. The top DLC layer was so thin that indenter came into multilayer film as applied load was less than 10 N which resulting in a high friction coefficient of about 0.45 accompanied with acoustic emission signal. Friction coefficient became steady as applied load increased to 43 N. Compared with that of B10 in Fig. 5a, a sharp decline of about 20 N can be observed from Fig. 12. Improving thickness ratio of (Cr, N)-DLC layer to DLC layer led to more macroparticles in multilayer films which deteriorated films' toughness. As indenter with an ever-increasing normal load touched multilayer film, cracks extended along with the boundary between macroparticles and multilayer film which made indenter easy to reach substrate surface and lowered multilayer film's adhesion strength (Fig. 13).

Friction coefficient of samples R2 and R4 measured by MS-T3000 is shown in Fig. 14a. During the first 70 min friction coefficient of sample R2 increased from 0.15 to 0.45 while that of sample R4 had a high value of about 0.3 after wear tests began. Friction coefficients of samples R2 and R4 fluctuated as wear tests went on due to the periodical structure of multilayer films. Due to the different composition and structure between DLC layer and (Cr, N)-DLC layer, friction coefficient of (Cr, N)-DLC layer is thought to be different with that of DLC layer. Al_2O_3 ball touched (Cr, N)-DLC layer and DLC layer alternatingly resulting in the periodical-changing friction coefficient. Two peaks can be found on the friction coefficient curve of sample R2 which indicated that depth of wear track was at least 350 nm (thickness of one bilayer in Fig. 10 is about 175 nm). While three peaks can be observed on the friction coefficient curve of sample R4 which indicated that depth of wear track was at least 525.

Average friction coefficient of multilayer films with different thickness ratios were calculated according to the friction coefficient during the whole wear tests, as shown in Fig. 14b. Compared with average friction coefficient of sample B10 (0.14), that of samples R2

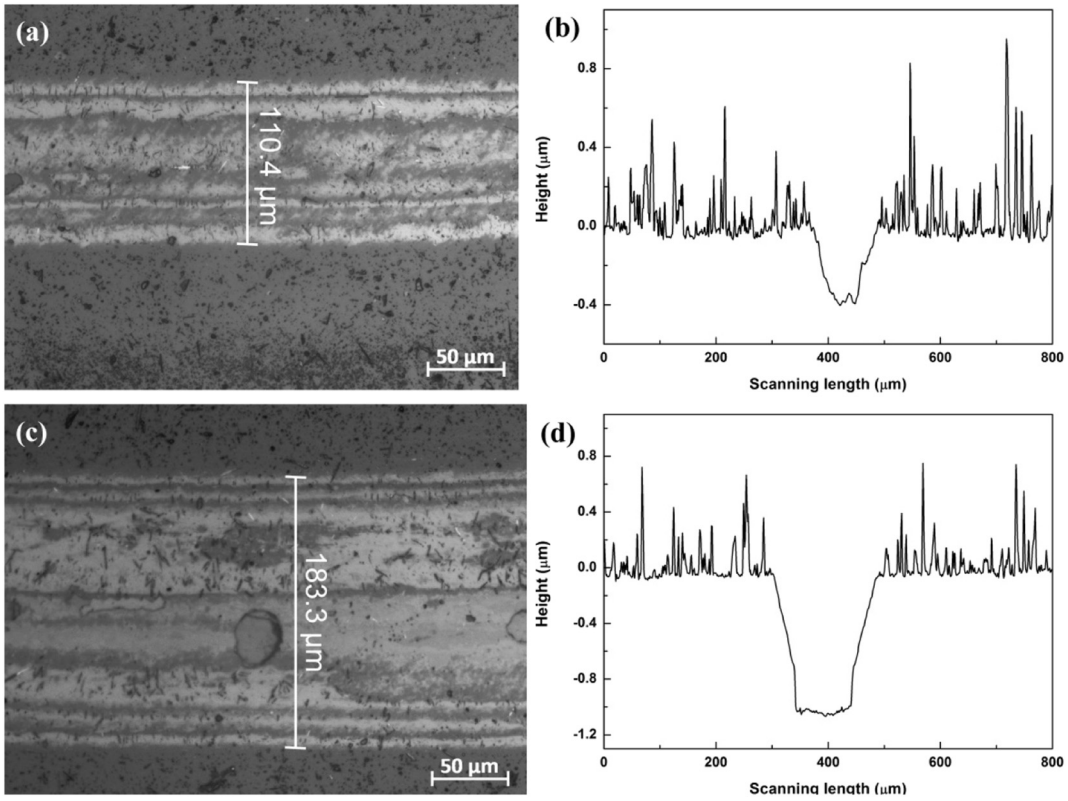

Fig. 16. Morphologies and profiles of wear tracks on (Cr, N)-DLC/DLC multilayer films: (a), (b) sample R2; (c), (d) sample R4.

and R4 (0.36 and 0.35, respectively) increased greatly. Friction coefficient of film has relationships with not only film roughness, but also film structure. DLC layer in samples R2 and R4 were too thin to lubricate the wear process giving rise to the high average friction coefficient.

Fig. 15 illustrates wear rates of multilayer films with different thickness ratios. Wear rates of samples B10 and R2 are 2.81×10^{-7} mm^3/Nm and 3.45×10^{-7} mm^3/Nm, respectively. Although average friction coefficient of sample R2 (0.36) is much higher than that of sample B10 (0.14), wear rate of sample R2 exceed that of sample B10 slightly. As for sample R4, wear rate is 1.23×10^{-6} mm^3/Nm which is several times the wear rates of samples B10 and R2. Too much macroparticles in sample R4 deteriorated film quality. Under the combined effect of normal load and friction force, cracks extended toward the interior of multilayer film. Macroparticles were much easier than atoms to be stripped from film, leading to the rise of wear rate. Besides, wear rate's standard deviation of sample R4 is much larger than that of samples B10 and R2. Given that wear rate was calculated according to cross-sectional areas of different positions in one wear track, the large standard deviation of sample R4 indicates the nonuniformity of abrasion.

Morphologies and profiles of wear tracks on samples R2 and R4 were investigated by an optical microscope and a surface profiler, respectively, as shown in Fig. 16. Width of wear track on sample R2 is 110.4 μm while that of sample R4 is much larger, up to 183.3 μm. In Fig. 16c, one pit with the diameter of about 37 μm on wear track can be seen apparently which were formed by macroparticles dropping, leading to the rise of wear rate. From Fig. 16b and d, depths of wear tracks on samples R2 and R4 are 0.4 μm and 1.0 μm, respectively. Fig. 10 shows that thickness of one bilayer is about 175 nm. On sample R2, the top two bilayers had been worn out and for sample R4, the top five bilayers had been worn out. Therefore, friction coefficient changed periodically during wear tests as shown in Fig. 14.

4. Conclusions

(Cr, N)-DLC/DLC multilayer films with different bilayer numbers and thickness ratios of (Cr, N)-DLC layer to DLC layer have been deposited on cemented carbides and Si wafers. Ra values of all (Cr, N)-DLC/DLC multilayer samples with a trend similar to the percentage of macroparticles on film surface are in the range of 37.8 nm to 108.8 nm. Quantity of macroparticles mainly derived from Cr target was affected by number of arc initiation, continuously arc-discharging time of targets and proportion of (Cr, N)-DLC layer. Alternating stress field from adjacent sublayers benefited the mechanical properties of multilayer films while macroparticles running through interfaces provided passages for cracks propagation and deteriorated films' mechanical properties. Average friction coefficient and roughness of multilayer films have the same changing trend and wear rates increased linearly from 2.45×10^{-7} mm^3/Nm to 3.81×10^{-7} mm^3/Nm when bilayer number rose from 10 to 20. As to multilayer sample with 10 bilayers, improving the proportion of (Cr, N)-DLC layer raised the quantity of macroparticles, leading to the increase of multilayer films' roughness, friction coefficient and wear rates.

Acknowledgments

This work was supported by GDAS' Project of Introducing Full-time Doctoral Degree Talent Support (No. 2018GDASCX-0948), Science and Technology Program of Guangzhou (No. 201607010091), Guangdong Science and Technology Program (No. 2017A070701027) and GDAS' Project of Science Technology Development (No. 2017GDASCX-0111).

References

[1] T. Ishikawa, J. Choi, The effect of microstructure on the tribological properties of a-C:H films, Diam. Relat. Mater. 89 (2018) 94–100.
[2] J. Robertson, Diamond-like amorphous carbon, Mater. Sci. Eng. R. Rep. 37 (2002) 129–281.
[3] W. Xu, K. Zhou, S. Lin, M. Dai, Q. Shi, C. Wei, Structural properties of hydrogenated Al-doped diamond-like carbon films fabricated by a hybrid plasma system, Diam. Relat. Mater. 87 (2018) 177–185.
[4] J. Vetter, 60years of DLC coatings: historical highlights and technical review of cathodic arc processes to synthesize various DLC types, and their evolution for industrial applications, Surf. Coat. Technol. 257 (2014) 213–240.
[5] D. Savchenko, V. Vorlíček, A. Prokhorov, E. Kalabukhova, J. Lančok, M. Jelínek, Raman and EPR spectroscopic studies of chromium-doped diamond-like carbon films, Diam. Relat. Mater. 83 (2018) 30–37.
[6] C. Bai, A. Liang, Z. Cao, L. Qiang, J. Zhang, Achieving a high adhesion and excellent wear resistance diamond-like carbon film coated on NBR rubber by Ar plasma pretreatment, Diam. Relat. Mater. 89 (2018) 84–93.
[7] C.P. Fenili, F.S. de Souza, G. Marin, S.M.H. Probst, C. Binder, A.N. Klein, Corrosion resistance of low-carbon steel modified by plasma nitriding and diamond-like carbon, Diam. Relat. Mater. 80 (2017) 153–161.
[8] D. Choudhury, T. Morita, Y. Sawae, J.M. Lackner, M. Towler, I. Krupka, A novel functional layered diamond like carbon coating for orthopedics applications, Diam. Relat. Mater. 61 (2016) 56–69.
[9] M. Jokari-Sheshdeh, F. Mahboubi, K. Dehghani, Structure and tribological behavior of diamond-like carbon coatings deposited on the martensitic stainless steel: the influence of gas composition and temperature, Diam. Relat. Mater. 81 (2018) 77–88.
[10] W. Dai, X. Gao, J. Liu, Q. Wang, Microstructure, mechanical property and thermal stability of diamond-like carbon coatings with Al, Cr and Si multi-doping, Diam. Relat. Mater. 70 (2016) 98–104.
[11] R.P.C. Costa, D.A. Lima-Oliveira, F.R. Marciano, A.O. Lobo, E.J. Corat, V.J. Trava-Airoldi, Comparative study of the tribological behavior under hybrid lubrication of diamond-like carbon films with different adhesion interfaces, Appl. Surf. Sci. 285 (2013) 645–648.
[12] C. Donnet, A. Erdemir, Tribology of Diamond-like Carbon Films: Fundamentals and Applications, Springer Science & Business Media, 2007.
[13] A.C. Ferrari, S.E. Rodil, J. Robertson, W.I. Milne, Is stress necessary to stabilise sp^3 bonding in diamond-like carbon, Diam. Relat. Mater. 11 (2002) 994–999.
[14] C.W. Zou, H.J. Wang, L. Feng, S.W. Xue, Effects of Cr concentrations on the microstructure, hardness, and temperature-dependent tribological properties of Cr-DLC coatings, Appl. Surf. Sci. 286 (2013) 137–141.
[15] M.C. Salvadori, F.S. Teixeira, W.W.R. Araújo, L.G. Sgubin, I.G. Brown, Interface tailoring for adhesion enhancement of diamond-like carbon thin films, Diam. Relat. Mater. 25 (2012) 8–12.
[16] Y. Lin, Z. Zhou, K.Y. Li, Improved wear resistance at high contact stresses of hydrogen-free diamond-like carbon coatings by carbon/carbon multilayer architecture, Appl. Surf. Sci. (2017) (in press).
[17] W. Dai, X. Gao, J. Liu, S.-H. Kwon, Q. Wang, Compositionally modulated multilayer diamond-like carbon coatings with AlTiSi multi-doping by reactive high power impulse magnetron sputtering, Appl. Surf. Sci. 425 (2017) 855–861.
[18] W. Dai, J. Liu, D. Geng, P. Guo, J. Zheng, Q. Wang, Microstructure and property of diamond-like carbon films with Al and Cr co-doping deposited using a hybrid beams system, Appl. Surf. Sci. 388 (2016) 503–509.
[19] C.Q. Guo, Z.L. Pei, D. Fan, R.D. Liu, J. Gong, C. Sun, Predicting multilayer film's residual stress from its monolayers, Mater. Des. 110 (2016) 858–864.
[20] O.V. Penkov, M. Khadem, J.-S. Lee, M. Kheradmandfard, C.-L. Kim, S.-W. Cho, D.-E. Kim, Highly durable and biocompatible periodical Si/DLC nanocomposite coatings, Nanoscale 10 (2018) 4852–4860.
[21] Z. Linan, W. Yanxia, Z. Shujiao, Y. Shengwang, T. Bin, L. Ying, Z. Bing, S. Yanyan, Influence of modulation periods on the tribological behavior of Si/a-C: H multilayer film, J. Phys. D. Appl. Phys. 51 (2018) 035302.
[22] Z. Xiaoyu, L. Zhibin, W. Guizhi, Z. Guangan, W. Liping, X. Qunji, Preparation and properties of DLC/MoS 2 multilayer coatings for high humidity tribology, Mater. Res. Express 3 (2016) 066401.
[23] M. Cui, J. Pu, G. Zhang, L. Wang, Q. Xue, The corrosion behaviors of multilayer diamond-like carbon coatings: influence of deposition periods and corrosive medium, RSC Adv. 6 (2016) 28570–28578.
[24] Z. Xu, H. Sun, Y. Leng, X. Li, W. Yang, N. Huang, Effect of modulation periods on the microstructure and mechanical properties of DLC/TiC multilayer films deposited by filtered cathodic vacuum arc method, Appl. Surf. Sci. 328 (2015) 319–324.
[25] Y. Lin, A.W. Zia, Z. Zhou, P.W. Shum, K.Y. Li, Development of diamond-like carbon (DLC) coatings with alternate soft and hard multilayer architecture for enhancing wear performance at high contact stress, Surf. Coat. Technol. 320 (2017) 7–12.
[26] F.-e. Yang, Y. Lu, R. Zhang, X.-h. Zhang, X.-h. Zheng, Microstructure and tribological properties of WSx/a-C multilayer films with various layer thickness ratios in different environments, Surf. Coat. Technol. 309 (2017) 187–194.
[27] Y.X. Xu, L. Chen, F. Pei, Y. Du, Structure and thermal properties of TiAlN/CrN multilayered coatings with various modulation ratios, Surf. Coat. Technol. 304 (2016) 512–518.
[28] Y. Wang, J.-W. Lee, J.-G. Duh, Mechanical strengthening in self-lubricating CrAlN/VN multilayer coatings for improved high-temperature tribological characteristics, Surf. Coat. Technol. 303 (2016) 12–17.
[29] X.D. He, L. Dong, J. Wu, D.J. Li, The influence of varied modulation ratios on crystallization and mechanical properties of nanoscale TiB_2/Al_2O_3 multilayers, Surf. Coat. Technol. (2018) (in press).
[30] C. Guo, Z. Pei, D. Fan, J. Gong, C. Sun, Microstructure and tribomechanical properties of (Cr, N)-DLC/DLC multilayer films deposited by a combination of filtered and direct cathodic vacuum arcs, Diam. Relat. Mater. 60 (2015) 66–74.

[31] P.J. Burnett, D.S. Rickerby, The mechanical properties of wear-resistant coatings: I: modelling of hardness behaviour, Thin Solid Films 148 (1987) 41–50.
[32] J. Musil, F. Kunc, H. Zeman, H. Polakova, Relationships between hardness, Young's modulus and elastic recovery in hard nanocomposite coatings, Surf. Coat. Technol. 154 (2002) 304–313.
[33] D.S. Bloom, J.W. Putman, N.J. Grant, Melting point and transformation of pure chromium, JOM 4 (1952) 626 (in press).
[34] R. Boxman, Macroparticle contamination in cathodic arc coatings: generation, transport and control, Surf. Coat. Technol. 52 (1992) 39–50.
[35] S. Shalev, R.L. Boxman, S. Goldsmith, Macroparticle dynamics during multi-cathode-spot vacuum arcs, IEEE Trans. Plasma Sci. 14 (1986) 59–62.
[36] J. Xu, L. Yu, Y. Azuma, T. Fujimoto, H. Umehara, I. Kojima, Thermal stress hardening of a-Si_3N_4/nc-TiN nanostructured multilayers, Appl. Phys. Lett. 81 (2002) 4139–4141.
[37] P. Kodali, K.C. Walter, M. Nastasi, Investigation of mechanical and tribological properties of amorphous diamond-like carbon coatings, Tribol. Int. 30 (1997) 591–598.
[38] B. Hammer, A.J. Perry, P. Laeng, P.A. Steinmann, The scratch test adhesion of TiC deposited industrially by chemical vapor-deposition on steel, Thin Solid Films 96 (1982) 45–51.
[39] P.K. Mehrotra, D.T. Quinto, Techniques for evaluating mechanical-properties of hard coatings, J. Vac. Sci. Technol. A 3 (1985) 2401–2405.
[40] A.G. Evans, Structural reliability - a processing-dependent phenomenon, J. Am. Ceram. Soc. 65 (1982) 127–137.
[41] Z. Fei, C.M. Suh, S.S. Kim, R.I. Murakami, Sliding-wear behavior of TiN- and CrN-coated 2024 aluminum alloy against an Al_2O_3 ball, Tribol. Lett. 13 (2002) 173–178.